ELECTRON EXCITATION CROSS SECTIONS FOR THE S II TRANSITIONS $3s^2 3p^3\ ^4S^0 \rightarrow 3s^2 3p^3\ ^2D^0, ^2P^0$ and $3s3P^4 4_P$

C. Liao, Steven J. Smith, D. Hitz[1], and A. Chutjian

Jet Propulsion Laboratory, California Institute of Technology

Pasadena, CA 91109

and

S. S. Tayal

Department of Physics

Clark Atlanta University, Atlanta, GA 30314

ABSTRACT

Experimental and theoretical collisional excitation cross sections are reported for the transitions $3s^2 3p^3\ ^4S^0 \rightarrow 3s^2 3p^3\ ^2D^0$, 2P" and $3s3p^4\ 4_P$ in *S II*. The transition wavelengths (energies) are 6716 Å (1.85 eV), 4069 Å (3.05 eV), and 1256 Å (9.87 eV), respectively. In the experiments, use is made of the energy-loss, merged-beams method. The metastable fraction of the *S II* beam was assessed and minimized. The contribution of elastically-scattered electrons was reduced by the use of lowered solenoidal magnetic field, use of a modulated radiofrequency voltage on the analyzing plates, and retarding grids to reject the elastically scattered electrons with larger Larrnor radii. For each transition, comparison , is made between experiment and the new 19-state R-matrix calculation.

[1] Permanent address: CEA/Département de Recherche Fondomentale sur la Matière Condensée, SI2A, 17 Rue des Martyrs, 38054 Grenoble Cedex 9, France

Subject headings: atomic data — ultraviolet: general

1. INTRODUCTION

Collisional excitation of singly-ionized sulfur is both an experimentally-challenging problem, and one that has direct relevance to the study of solar (Feldman, Doschek, VanHoosier, & Purcell 1976), stellar (Espey e? a/. 1994), and solar-system objects, especially the Io-Jupiter torus (Hall *et a/. 1994;* Shemansky 1988). In any assessment of the conditions of an astronomical plasma (electron temperature, electron and ion densities), the two important quantities required are the electron collisional rate coefficient $C(g \rightarrow i)$ and the spontaneous radiative decay rate $A(i \rightarrow g)$ between ground g and excited i levels. The C/g $\rightarrow i)$ are integrals of the collision strength (or excitation cross section) for the transition, taken over an electron energy distribution function (usually Maxwellian) (Ramsbottom, Bell, & Stafford 1996). For almost every ion, charge-state, and transition of astrophysical interest, the $C(g \rightarrow i)$ are derived from *calculated* collision strengths, with practically no *experiments/* measurements to verify or calibrate theory (see, for example, discussions in Lang 1994

Reported herein are first measurements of excitation cross sections for the transitions $3s^2 3p^3\ ^4S^0 \rightarrow 3s^2 3p^3\ ^2D^o$, 2P" and $3s3p^4\ ^4P$ in *S II*. A partial energy-level diagram is given in Figure 1, This study is part of a larger planned effort to measure collision strengths in a number of charge states of sulfur and oxygen present in the 10 ' torus. The measurements are made using the electron energy-loss, merged-beams method (Zuo e? *a/.* 1995, Smith *et a/.* 1996, Dunn *et a/.* 1995). The measurements are absolute except for a small correction above threshold, made from an accurate theoretical calculation (Manson 1969), of the contribution of elastic scattering from

S II to the inelastic scattering. In order to assess theory, also reported herein are results in a new 19-state R-matrix calculation, as well as comparisons with two previous close-coupling calculations (Cai & Pradhan 1993; Tayal, Henry, & Nakazaki 1987). A consistency check is also made with the effective collisions strengths $C(g \rightarrow i)$ reported in a recent 18-state *R*-matrix calculation by Ramsbottom, Bell, & Stafford (1996).

Experimental details unique to the e-S II measurements are given in § 2. The theoretical R-matrix approach is described in § 3, and experimental cross sections compared with theory are given in § 4.

2. EXPERIMENTAL METHODS

The basic experimental approach used is the same as in previous work on e-C II scattering (Smith e? *a/. 1996),* and only differences will be noted here. The basic equation relating the experimental parameters to the final excitation cross section *u(EJ* is given by,

$$\sigma(E) = \frac{R e^2 \mathcal{F}}{\epsilon I_i I_e L} \left| \frac{v_e v_i}{v_e - v_i} \right| , \qquad (1)$$

where *R* is the total signal rate (s-l), e the electron charge, I_e and Ii the electron and ion currents (A), respectively, v_e and vi are the electron and ion velocities (cm S-l), respectively, *L* the merged path length (cm), ϵ the efficiency of the grids-microchannel plate detection system (dimensionless), $\mathcal{F}$ the overlap factor between the electron and ion beams (cm^2), and $\sigma(E)$ the excitation cross section (cm^2).

2.1. Determination of the Metastable Fraction in the S//Beam

Ion sources which generate beams of singly- or multiply-charged ions often produce a non-negligible fraction *f* of ions in metastable states, These ions are counted in the total ion current /j in equation (1), but do not contribute to the energy-loss signal rate *R.* Hence, the measured cross section is lower than its true value by a factor 1 /(l-f). Possible metastable levels in *S //* are ^{2}D, ^{2}P" which are prevented from optical decay to the $^4S^0$ ground state by parity and/or angular-momentum violation. Population in these two levels will depend upon details of ion formation [discharge voltage and current, feed-gas pressure, microwave power in the case of electron-cyclotron resonance (ECR) multiply-charged ion sources], in ion transit time to the collision region, or ion storage time prior to study (for ion storage rings).

In the present case *S //* was generated in a Colutron DC-discharge ion source with CS_2 used as the feed gas. To prevent contamination by any $^{16}O_2^+$ with ^{32}S *//*, the isotope ^{34}S *//* was resolved by the charge-analyzing magnet, and only this isotope was used in all studies. As in previous work, the metastable S *//* fraction was measured using the beam-attenuation method (Zuo *et al. 1995,* Smith et *a/. 1996),* Here one relies on the fact that charge exchange from a metastable ionic state will very likely proceed with a significantly different (usually larger) cross section than that for exchange from the ground ionic state. Attenuation of a 6 keV beam of S *//* was studied as a function of N_2 pressure in the extraction beam line. Results are shown in Figure 2 for two cases where the ion source was run at (a) a low anode voltage and low filament current, and (b) a high anode voltage and filament current. One notes in Figure 2 a region of two

slopes, with a break at approximately 1.0 in the relative N_2 pressure scale. This is indicative of a metastable state(s) undergoing charge transfer with larger cross section. In case (a) there is no break, indicating the absence of metastable states, and only the ground state is attenuated by charge transfer. In all data reported herein, the ion source was run under case (a) conditions, with a metastable fraction and estimated error of $f = 0.00^{+0.02}_{-0.00}$.

2.2 Overlapping Elastic and Energy-Loss Transitions

As was noted for C *II*, use of a trochoidal deflector and retarding grids can still give contributions from elastically-scattered electrons at large scattering angles, and from inelastically-scattered electrons from other nearby transitions. Given the resolution of the trochoidal deflector, and referring to the energy-level diagram in Figure 1, one sees that excitation of the $^4S^0 \rightarrow {}^2P^\circ$ transition at a center-of-mass (cm,) energy of 4 eV can contain contribution from the $^4S^0 + {}^2D$" transition, and from large-angle elastically-scattered electrons.

Two approaches were employed herein to prevent the large-angle, elastically-scattered electrons from entering the analyzer plates. The first was to carry out measurements at a lowered magnetic field, and the second was to use a radio-frequency (RF) potential across the analyzing plates. When judiciously applied, these methods can prevent nearly all elastically-scattered electrons from contributing to the inelastic signal. The two methods were employed in acquiring the second (later) half of the collected data set. For the first half of the collected data, only the retarding-grids method for

limiting the elastic and inelastic overlaps was used (see Smith *et al.* 1996, Zuo *et al.* 1995, Smith *et al. 1993* for C *II*, O *II* and *Mg II*, respectively). Using the grids, the contribution from large-angle elastic scattering will depend on a number of experiment.al parameters: the solenoidal magnetic field, analyzer-plate voltages, laboratory (LAB) -to-c.m. angle transformation, chosen potentials on retarding grids, and the selected region of interest (ROI) on the position-sensitive detector (PSD).

Electron trajectory calculations using the 3-D SIMION computer code (Dahl 1995) were used to estimate the size of the inelastic contribution from competing channels and to calculate the non-negligible fraction *F* of elastically-scattered electrons which could strike the PSD under given tuning conditions. The contribution of inelastic-scattering signal from competing channels was found to be negligible in the present case. Only a small range of laboratory polar (ϑ) and azimuthal (φ) elastic scattering actually contribute to the fraction *F,* A complete set of trajectories for each impact energy and polar scattering angle was calculated, In our past work, the elastic differential scattering cross section (DCS) was approximated by using the Rutherford e-*H II* DCS. However, the S *II* elastic DCS was expected to show partial-wave interference structure, which can vary with incident electron energy. Hence in the present work the elastic DCS was calculated at each CM energy, and for each angle ϑ, by interpolation of the partial-wave components calculated by Manson (1 969) for *Si II* (Z= 14) and *Ar II* (Z= 18), Partial s-, *p*-, *d*-, and *f*-wave phase shifts as a function of energy for S *II* (Z= 16) were then interpolated from the calculations for *Si II* and *Ar II* since there was a smooth progression between these two. Results are shown in Figure 3 for the range of energies relevant to the present work. Also shown for comparison is the Rutherford (e-if*II*) elastic DCS

which shows none of the interference phenomena.

For a given impact energy, and at each ϑ, the product of the fraction F and the DCS at that ϑ is calculated, The products are summed over all ϑ to give the total elastic contribution at that energy, This contribution is then used in the base-line subtraction method as described in the previous work. Stated briefly, retarding grids were used to make a "low" (all signal collected) and "high" (only energetic, low-angle elastic scattering collected) electrostatic retard measurements. The net difference signal is the inelastic signal plus a calculated fraction F of the large-angle elastic scattering. The "zero" base line is incremented sequentially so that a running sum of the total counts above and below the baseline are monitored. The baseline selection is halted when the total number counts that lie below the adjusted baseline equals the expected fraction of elastic scattering. The inelastic signal is taken as the total number of counts that lie above this newly-adjusted baseline, This method effectively subtracts the fraction F of elastically-scattered electron signal from the total inelastic signal.

As pointed out above, two methods were employed in the second half of the data set to limit the acceptance of large-angle, elastically-scattered electrons, In one new method a radio-frequency (RF) potential was applied across the analyzing plates (labeled AP, see Figure 2 of Zuo et *a/.* 1995). Electrons spiraling about the solenoidal B field will have their orbital dimensions increased, depending on the match between the RF and the Larmor frequencies, and the amplitude of the RF potential. Approximately one-fourth of the data was acquired with the RF fields method. Typical operating conditions for a 50 gauss solenoidal field were RF frequency of 139.8 MHz and peak voltage of 15 V. This voltage was impressed on the normal DC deflection voltage of the trochoidal analyzing

plates. Comparisons at several energies were made between the RF fields method, and the earlier baseline subtraction method. Agreement between the methods was within the range of experimental accuracy quoted herein.

The method using lowered magnetic fields was used during the last quarter of the data acquisition, The solenoidal field was changed from 50 gauss to 25 gauss. This causes the high-angle, elastically- scattered electrons to have proportionately larger Larmor radii. These radii can exceed the opening dimension of the analyzer plate, in which case the analyzer plates themselves act as defining apertures: the plates limit transmission of the large-angle, elastically-scattered electrons, and transmit inelastically-scattered electrons, since the latter have less perpendicular velocity and therefore a smaller Larmor radius in the magnetic field.

3. COLLISION CALCULATIONS

Electron collisional excitation cross sections for the forbidden $3s^2 3p^3 4S0 \rightarrow 3s^2 3p^3$ ^2D", 2P" and resonance $3s3p^4 4_p$ transitions in S // are calculated in a 19-state close-coupling approximation using the opacity R-matrix codes (Barrington e? *a/ 1987).* Nineteen LS target states were considered in the close-coupling expansion: $3s^2 3p^3$ $^4S^o, ^2D^o, ^2P^o$; $3s3p^4$ $^4P, ^2D, ^2S$; $3s^2 3p^2 3d$ $^2P, ^4F, ^4D, ^2F, ^4P$; $3s^2 3p^2 4s$ $^4P, ^2P$; and $3s^2 3p^2 4p$ $^2S^o, ^4D^o, ^4P^o, ^2D^o, ^4S^o, ^2P^o$. These states are represented by extensive configuration-interaction (Cl) wavefunctions. Ten orthogonal one-electron radial functions are chosen as the Hartree-Fock (HF) functions of the $3s^2 3p^3 {}^4S^o$ ground state given by Clementi and Roetti (1 974), while other functions have been obtained by optimizing the energy

differences and oscillator strengths among the target states using the general structure code CIV3 (Hibbert 1975), The wavefunctions used in this study are to some extent similar to those of Ojha & Hibbert (1 989) and Ramsbottom, Bell & Stafford (1996). The 3d, 4s, and 4p functions are chosen of spectroscopic type, and are optimized on the excited states $3s^2 3p^2 3d$ 4P, $3s^2 3p^2 4s$ 4P, and $3s^2 3p^3 4p$ 4P", respectively, The 4d and 4f functions are correlation type, and are obtained to improve the energies of the $3s3p^4$ 4_P and $3s^2 3p^2 3d$ 4_P states, respectively. The radial part of each one-electron function is represented as a sum of Slater-type functions,

$$P_{nl} = \sum_{j=1}^{k} C_{jnl} r^{l_{jnl}} \exp(-\xi_{jnl}) , \qquad (2)$$

where n and l are, respectively, the principal and orbital quantum numbers; and C_{jnl}, ξ_{jnl}, and l_{jnl} are expansion coefficients, exponents, and powers of the radial distance r, respectively. The parameters of the optimized radial wavefunctions are given in Table 1. In obtaining these functions we have chosen $k > n-l$, which implies that the coefficients $C_{j..}$ are determined by orthonormality as well as by variational considerations. This improves the flexibility of the functions to give a good representation of the target states. Several calculations were carried out to test the convergence of the Cl expansions for different LS symmetries. Up to two-electron excitations were considered from the basic configurations $3s^2 3p^3$, $3s3p^4$, $3s^2 3p^2 3d$, $3s^2 3p^2 4s$, and $3s^2 3p^2 4p$. All configurations with weight greater than 0.008 are retained in the final calculation, Presented in Table 2 are calculated excitation energies of the various states relative to the ground state. These are compared with the experimental energies given by Petterson (1 983); and with the theoretical energies reported by

Ramsbottom, Bell, & Stafford (1 996) and Cai & Pradhan (1 993). The present calculated energies agree to better than 4% with the measured values for most of the excited states. The largest discrepancies are for the $3s^2 3p^3\ ^2D$" and 2P" states where calculated results differ from experiment by about 14°A and 13%, respectively. it should be noted that Cai & Pradhan (1 993) did not get the order of the $3s^2 3p^2 3d\ 4_D$ and 2_F states correct, and their calculated energies for these states do not agree well with experiment and other calculations, It is perhaps an indication of the poor quality of the 3d function in their calculation. The scattering wavefunction representing the electron-S // collision was expanded in terms of the R-matrix basis functions

$$\Psi_k = A\sum_{ij} a_{ijk}\Phi_i\,(1,2,...15;\, r_{16}\,\sigma_{16})\,u_j(r_{16}) + \sum_j b_{jk}\phi_j(1,2,...16) \qquad (3)$$

where the Φ_i are channel functions formed by coupling the multiconfiguration target wavefunctions with the angular and spin parts of the wavefunctions for the scattered electron. The u_i are continuum basis functions which represent the motion of the scattered electron. Twenty five continuum functions were used in each channel. The diagonal elements of the inner-region Hamiltonian matrix were adjusted before diagonalization to reproduce observed energies of the target states. Cross sections were obtained for angular momenta L in the range L = O to 11. These partial waves gave converged cross sections for all three transitions considered here. An energy mesh of 0.001 Ry was chosen for the scattering calculation in the threshold energy region, which allowed resolution of the complicated resonance structure in the excitation cross section,

4. RESULTS AND DISCUSSION

4.1 Experimental and Theoretical Results for the $^4S^0 + {}^2D^0$ Excitation

Experimental and theoretical cross sections for the first forbidden $^4S^0 \rightarrow {}^2D^o$ transition are shown in Figure 4 and Table 3. The experimental errors are quoted at the 90% confidence level, or 1,7 standard deviations of the mean (σ). The experimental cross sections are measured up to 6.0 eV (3,2 x threshold), and are displayed as solid circles in the figure, The theories in Figure 4 are the present R-matrix calculation, an earlier 12-state calculation by Cai & Pradhan (1 993), and a 6-state calculation by Tayal, Henry, & Nakazaki (1 987). The theoretical cross sections show complicated, sharp resonance structures which cannot be resolved in the measurements with a 250 meV electron-energy width, For comparison, therefore, results in Figure 4 for the three theories have been convoluted with a Gaussian electron-energy distribution of 250 meV FWHM. As can be seen from Figure 4 there is good accord between experiment and the three theories over the energy range studied. There is also good agreement among the three theories but some discrepancies exist in the magnitude of cross section. For example, there is excellent agreement in prediction of the peak of the cross section (at about 2.1 eV), but the magnitudes at the peak differ by up to 250A, This is perhaps caused by the difference in wavefunction used in the three calculations,

Direct comparison for any of the transitions to the theory of Ramsbottom, Bell, & Stafford (1 996) was not possible since only effective collisions strengths were reported therein, However, Tayal (1 996) has Calculated effective collision strengths from the

present 19-state cross sections by averaging over a Maxwellian electron-energy distribution. Good agreement was found with the calculated effective collision strengths of Ramsbottom, Bell, & Stafford (1 996).

4.2 Experimental and Theoretical Results for the $^4S^0 \rightarrow$ 2P" Excitation

Experimental and theoretical calculations for the $^4S^0 \rightarrow$ 2P" excitation are shown in Figure 5. Experimental data are measured up to 1.64 x threshold, Three calculations are again available: the present 19-state R-matrix, the 12-state F?-matrix (Cai and Pradhan 1993), and the 6-state close-coupling (Tayal, Henry, & Nakazaki 1987), The three theories have been convoluted with a 250 meV electron-energy width to conform to the experimental measurements, There is excellent agreement between the present 19-state calculation and experiment. However, the three calculations differ substantially from one another, particularly in the near-threshold range 3-4 eV. At 3.5 eV there is about a factor of two disagreement between the 19-state and 6-state calculations, while the results of Cai and Pradhan (1 993) are a factor of about 2.7 lower than the 19-state calculation and experiment. The threshold peak is quite broad in the calculation of Cai & Pradhan relative to the shape of the present theory. Differences among the three calculations at threshold are surprising, and are indicative of the sensitivity of the resonance structure to details of wavefunctions and electron-correlation terms. Experimental results support the present 19-state calculation.

The effective collision strengths for the $^4S^0 \rightarrow {}^2P^0$ transition calculated from the

present 19-state calculation are well within 20960 f the recent 18-state calculations of Ramsbottom, Bell, & Stafford (1 996), again in support of the 19-state calculation (see Tayal 1996). Present experimental and theoretical cross sections are listed in Table 4.

4.3 Experimental and Theoretical Results for the $^4S^0 \rightarrow 4_P$ Excitation

Experimental results for the $^4S^0 \rightarrow 4_P$ resonance excitation are shown in Figure 6 to an energy of 1.3 x threshold. These are compared with the present 19-state calculation and the 12-state calculation (Cai & Pradhan 1993), both convoluted to the experimental energy spread. The cross section at the lowest available energy (0.5 au or 13.6 eV) from the 6-state calculation (Tayal, Henry, & Nakazaki 1987) is also shown (solid square). One sees overall good agreement between experiment and the present 19-state calculation, and with the 0,5 au-calculation. Tayal (1 996) also finds reasonable agreement in terms of effective collisions strengths between the 19-state and 18-state (Ramsbottom, Bell, & Stafford 1996) calculations.

As seen in Figure 6 the results of Cai & Pradhan (1 993) are a factor of about 1.5 smaller than the 19-state calculation and experiment in the threshold region from 9.9 to 11 eV; and smaller than the 19-state calculation at energies above 13 eV. Tayal (1 996) noted substantial disagreement between the 19-state and 12-state calculations in the magnitude, shape, and position of resonances, This was attributed to the poor quality of the 3d functions in the 12-state calculation (Cai & Pradhan 1993), Experimental and present 19-state convoluted cross section are given in Table 5 in the energy range 9.5-

12.8 eV.

5. SUMMARY

The first experimental cross sections for excitation from the S// ground $^4S^0$ state to the lowest three excited $^2D^0$, $^2P^0$ and 4_p states have been measured using the energy-loss, merged-beams technique in the near-threshold regions. These are compared with the present 19-state R-matrix calculation, and with other available calculations. There is very good agreement between experiment and the theory, providing support to the validity of the present calculations. Significant differences are noted in the energy range considered here between the present theory, that of Cai & pradhan (1993), and Tayal, Henry, & Nakazaki (1 987), particularly for the forbidden $^4S^\circ \rightarrow 2P^o$ and the resonance $^4S^0 \rightarrow 4_p$ transitions.

We thank 1. D. Williams for calculating angular differential elastic-scattering cross sections for *S II*, and A, K, Pradhan for the electronic transmission of his data files. C. L. and D. H. thank the National Academy of Sciences-National Research Council for support at JPL. S, S. T. acknowledges support from the National Aeronautics and Space Administration under the Planetary Atmospheres Program, The calculations were performed on the JPL/Caltech Cray Supercomputer. The experimental work was carried out at the Jet Propulsion Laboratory, California Institute of Technology, and was supported by NASA.

REFERENCES

Barrington, K.A., Burke, P. G., Butler, K., Seaton, M. J., Storey, P. J., Taylor, K. T., & Yu Yan 1987, J. *Phys. B, 20, 6379*

Cai, W. & Pradhan, A. K. 1993, *ApJS, 88, 329*

Clementi, E. & Roetti, C. 1974, *Atom. Data Nucl. Data Tables 14,* 177

Dahl, D. A, 1995, *SIMION* 3D *Version 6.0 User's Manual,* Idaho National Engineering Laboratory Report No. INEL-95/0403

Dunn, G. H., Djurić, N., Chung, Y-S., Bannister, M., & Smith A. C. H. 1995, *Nucl. Instr. Methods, B 98, 107*

Espey, *et al. 1994, ApJ, 434, 484*

Feldman, U., Doschek, G. A., VanHoosier, M. E., & Purcell, J. D. 1976, *ApJs 31, 445*

Hall, D. T., *et al.* 1994, *ApJ, 426, L51,*

Hibbert, A. 1975, *Comput. Phys. Commun., 9,* 141

Lang J. 1994, *At. Data Nucl. Data Tables, 57,* 1

Ojha, P. G. & Hibbert, A. 1989, *J. Phys. B, 22,* 1153

Manson, S. T., 1969, *Phys. Rev., 782, 97.*

Petterson, J. E. 1983, *Phys. Scripts, 28, 421*

Ramsbottom, C.A., Bell, K. L., & Stafford, R, P, 1996, *At. Data Nut/. Data Tab/es, 63,* 57.

Shemansky, D.E. 1988, *J. Geophys. Res., 93, 1773.*

Smith, S.J., *et a/. 1993, Phys. Rev. A, 48, 292.*

Smith, S. J., Zuo, M., Chutjian, A., Tayal, S. S., & Williams, 1. D. 1996, *ApJ, 463, 808*

Tayal, S. S. 1996, *ApJ* (to be submitted)

Tayal, S. S., Henry, R. J.W., and Nakazaki, S. 1987, *ApJ, 373, 487*

Zuo, M., Smith, S. J., Chutjian, Williams, 1. D., Tayal, S. S., & McLaughlin, B. M. 1995, *ApJ, 440, 421*

TABLE 1

Values of Slater-Type Parameters of the Radial Functions

Orbital	c_{jnl}	n_{jnl}	ξ_{jnl}	Orbital	c_{jnl}	n_{jnl}	ξ_{jnl}
3d	0.12049	3	2.57781	4d	0.02094	3	6.30185
	0.00739	3	6.36475		0.87831	3	1.85553
	0.29657	4	1.48870		0.19514	4	1,43842
	0.72934	4	0.83515		-0.73406	4	0.82270
4s	-0.03635	1	15,55697	4f	1.07429	4	2,23484
	1,39720	2	1,24030		-0.59092	4	2.40099
	-1,38272	3	1.85274		0.48372	5	1,45095
	0.07303	3	9.29793		0.15286	5	1.02484
	-0.32118	4	3.82525				
	0,83069	4	0,97430				
4p	0,12550	2	5.20582				
	-0.27200	3	2.53721				
	-0.45324	3	1.04197				
	1.11759	4	0.96194				
	0.25820	4	0.67794				

TABLE 2

Calculated and Experimental Energy Levels (in eV) of S II

Index	State	Energy			
		Present	RBS	CP	Experiment
1	$3s^2 3p^3\ {}^4S^o$	0.0000	0.0000	0.0000	0.0000
2	$3s^2 3p^3\ {}^2D^o$	2,1092	2.1326	1.9987	1.8439
3	$3s^2 3p^3\ {}^2P^o$	3.4319	3.4545	3,2749	3.0447
4	$3s3p^4\ {}^4P$	9.9061	9,7396	9.8057	9.8705
5	$3s3p^4\ {}^2D$	12.3845	12,4183	12.6398	12,1391
6	$3s^2 3p^2 3d\ {}^2P$	13.3457	13.4940	13,8493	13.1111
7	$3s^2 3p^2 4s\ {}^4P$	14.1356	13,6967	14.4344	13.6390
8	$3s^2 3p^2 3d\ {}^4F$	14.1508	14.0842	14,6480	13.7019
9	$3s^2 3p^2 4s\ {}^2P$	14.5979	14.2017	15.1405	14.0458
10	$3s^2 3p^2 3d\ {}^4D$	14.6820	14,5081	17.2834	14.1636
11	$3s^2 3p^2 3d\ {}^2F$	14.8374	14,8053	17,2834	14,2681
12	$3s3p^4\ {}^2S$	15,1764	15.2175	15.4222	14,8515
13	$3s^2 3p^2 4p\ {}^2S^o$	15.8788	15,6151		15.5582
14	$3s^2 3p^2 4p\ {}^4D^o$	16.3874	16.0748		15.9057
15	$3s^2 3p^2 4p\ {}^4P''$	16.5210	16.2910		16,1161
16	$3s^2 3p^2 3d\ {}^4P$	16.5803	16.4448		16.2089
17	$3s^2 3p^2 4p\ {}^2D''$	16.8051			16.2382
18	$3s^2 3p^2 4p\ {}^4S^o$	16.5923			16.2456
19	$3s^2 3p^2 4p\ {}^2P^o$	17,1136			16.5343

RBS: Ramsbottom, **Bell & Stafford (1 996)**

CP: Cai & Pradhan (1993)

Experiment: Petterson (1 983)

Table 3

Experimental and Theoretical (}?-matrix) Cross Sections $\sigma(E)$ for the $^4S^o \rightarrow {}^2D^o$ (Forbidden) Transition in S II

Experimental		R-matrix
Energy (eV)	σ(E)	σ(E)
1.6	-0.10[†]	0.00[†]
1.7_5	2.25[†]	2.42[†]
1.9	5.78	8.24
2.0	7.60	11.3
2,3	10,5	10,6
2,5	6,68	9.30
2.7	10.0	8.22
3.0	5.33	6,46
3.5	6.29	4,08
4.0	3.72	3.57
4.5	3.54	3,40
5.0	3,61	3.21
6,0	2.03	2.84

Notes.— In Tables 3-5 theoretical results have been convoluted with a 250 meV (FWHM) energy width. Units of cross sections are 10^{-16} cm^2.

[†] Non-zero values in experiment and theory below threshold (as elsewhere) include effects of the electron-energy spread in the experiments.

Table 4

Experimental and Theoretical (R-matrix) Cross Sections $\sigma(E)$ for the $^4S^o \rightarrow {}^2P^o$ (Forbidden) Transition in S II

Experimental		R-matrix
Energy (eV)	u(E)	u(E)
2.8	0.33'	0.01[1]
2.9	0.19'	0.33[+]
3.0	1.17	0.98
3.3	2.34	3.41
3.5	*3,71*	3,97
3.7_5	*3.00*	3.74
4.0	*2.55*	3.08
4.5	*1.93*	2,08
5,0	*1.67*	1,58

Table 5

Experimental and Theoretical (R-matrix) Cross Sections $\sigma(E)$ for the $^4S^o \rightarrow 4_p$ (Resonance Allowed) Transition in S II

Experimental		R-matrix
Energy (eV)	u(E)	u(E)
9.5	-0,11′	0.00′
9.6	0.19†	*0.04′*
9.7_5	*0,26′*	0.49†
9.8	*0.09′*	0.84†
9.8_5	*1.47*	*1.26*
9.9	*1,01*	*1.69*
10.0	*2.88*	*2.34*
10.2	*3.18*	*2.46*
10.4	*2,35*	*2.28*
10.5	*2.16*	*2.25*
10.7	*2,47*	*2.08*
10.8_5	*1.65*	*1.95*
11.0	*1.48*	*1.77*
11.2	*2.08*	*1.58*
11.3	*2.28*	*1.54*
11.4	*1.68*	*1.50*
11.6	*1.51*	*1.44*
11.7_5	*0.99*	*1,40*
12.0	*1.79*	*1.23*
12.2	*1,40*	*1.24*
12.5	*1.76*	*1.31*
12.8	*1.67*	*1.26*

FIGURE CAPTIONS

Figure 1 Partial energy-level diagram for S II, showing the $3s^2 3p^3\ ^4S^0 \rightarrow 3s^2 3p^3$ 'D", $^2P^0$ (forbidden) and $3s^2 3p^3\ ^4S^0 + 3s3p^4$, $3p^2 4s$, $3p^3 3d$ 4_p (allowed) transitions.

Figure 2 Attenuation curve measured for a 4.0 keV beam of S II in N_2. The source of S II was CS_2. Conditions are shown for (a) low anode voltage and low filament current, and (b) high anode voltage current and high filament curent. The metastable fraction shown here is f = 0.13, and was 0.00-0.02 for the data reported herein.

Figure 3 Calculated elastic differential cross sections (DCS) for e-S II scattering. The DCS were obtained from summed partial waves interpolated from the results of Manson (1 969). Collision energies are indicated on each curve, Also shown for comparison is the Rutherford DCS R(5.0) at 5.0 eV energy.

Figure 4 Experimental (filled circles) and theoretical cross sections for excitation of the $^4S^0 \rightarrow {}^2D^0$ transition in S II. Theoretical results are convoluted with a 250 meV (FWHM) electron-energy width: solid line, present 19-state R-matrix calculation; dashed line, Cai & Pradhan (1 993) 12-state R-matrix calculation; dotted line, Tayal, Henry, & , Nakazaki (1 987) 6-state R-matrix calculation.

Figure 5 **Experimental (filled circles) and theoretical cross sections for excitation of the $^4S^o \rightarrow$ 2P" transition in *S II*. Theoretical results are convoluted with a 250** meV (FWHM) electron-energy width. Notation for the theories is the same as in Fig. 4.

Figure 6 **Experimental (filled circles) and theoretical cross sections for excitation of** the $^4S^0 + 4_P$ transition in *S II*. Theoretical results are convoluted with a **250** meV (FWHM) electron-energy width. Notation for the theories is the same as in **Fig. 4, except that the solid square represents the calculation of** Tayal, Henry, & Nakazaki (1 987).

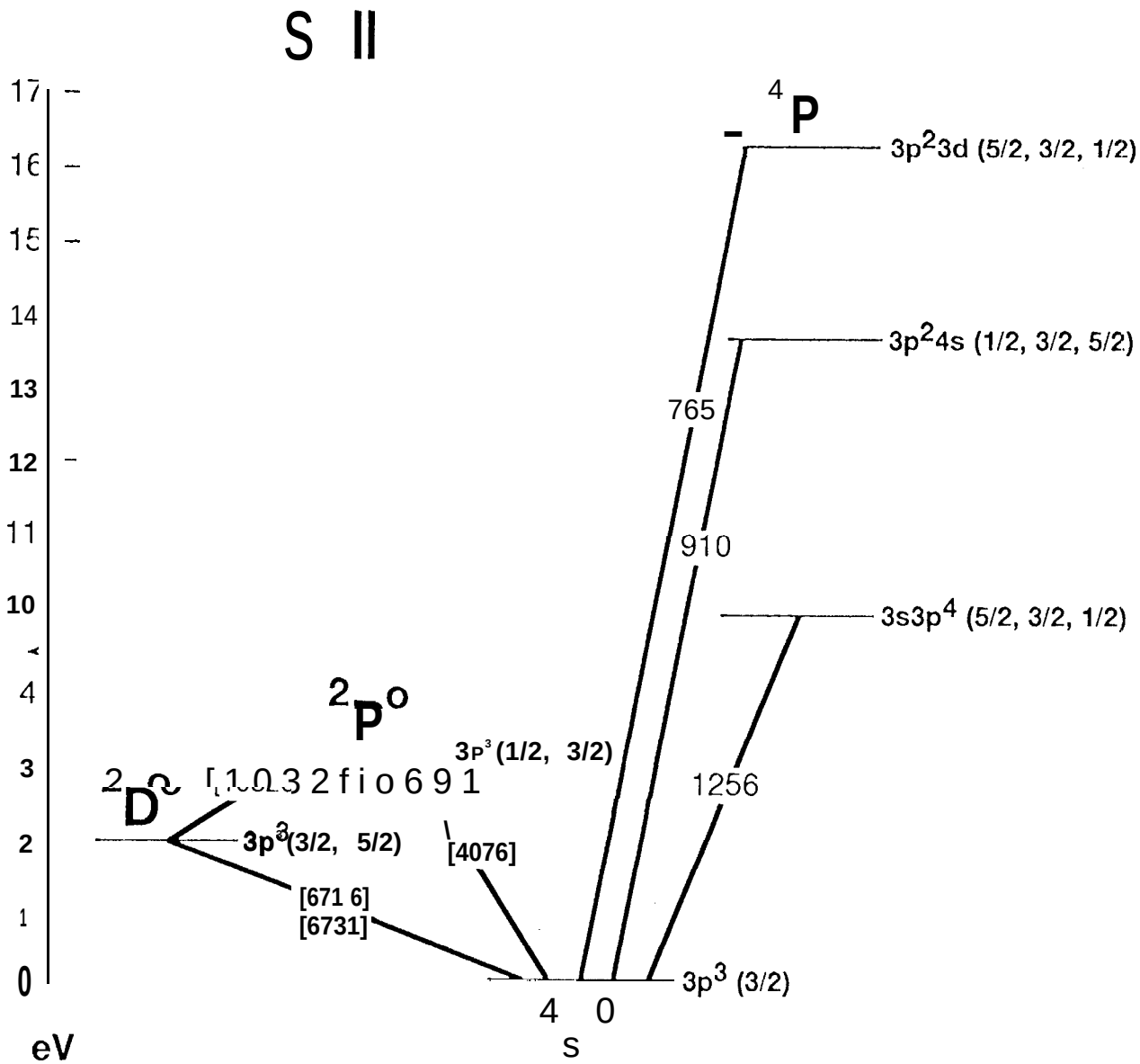
S II
17
16
15
14
13
12
11
10
4
3
2
1
0
eV
^4P
$3p^2 3d$ (5/2, 3/2, 1/2)
$3p^2 4s$ (1/2, 3/2, 5/2)
765
910
$3s3p^4$ (5/2, 3/2, 1/2)
$^2P^o$
$3P^3$ (1/2, 3/2)
$^2D^o$
[1032 fio691
$3p^3$ (3/2, 5/2)
[4076]
1256
[671 6]
[6731]
$3p^3$ (3/2)
4 0
S

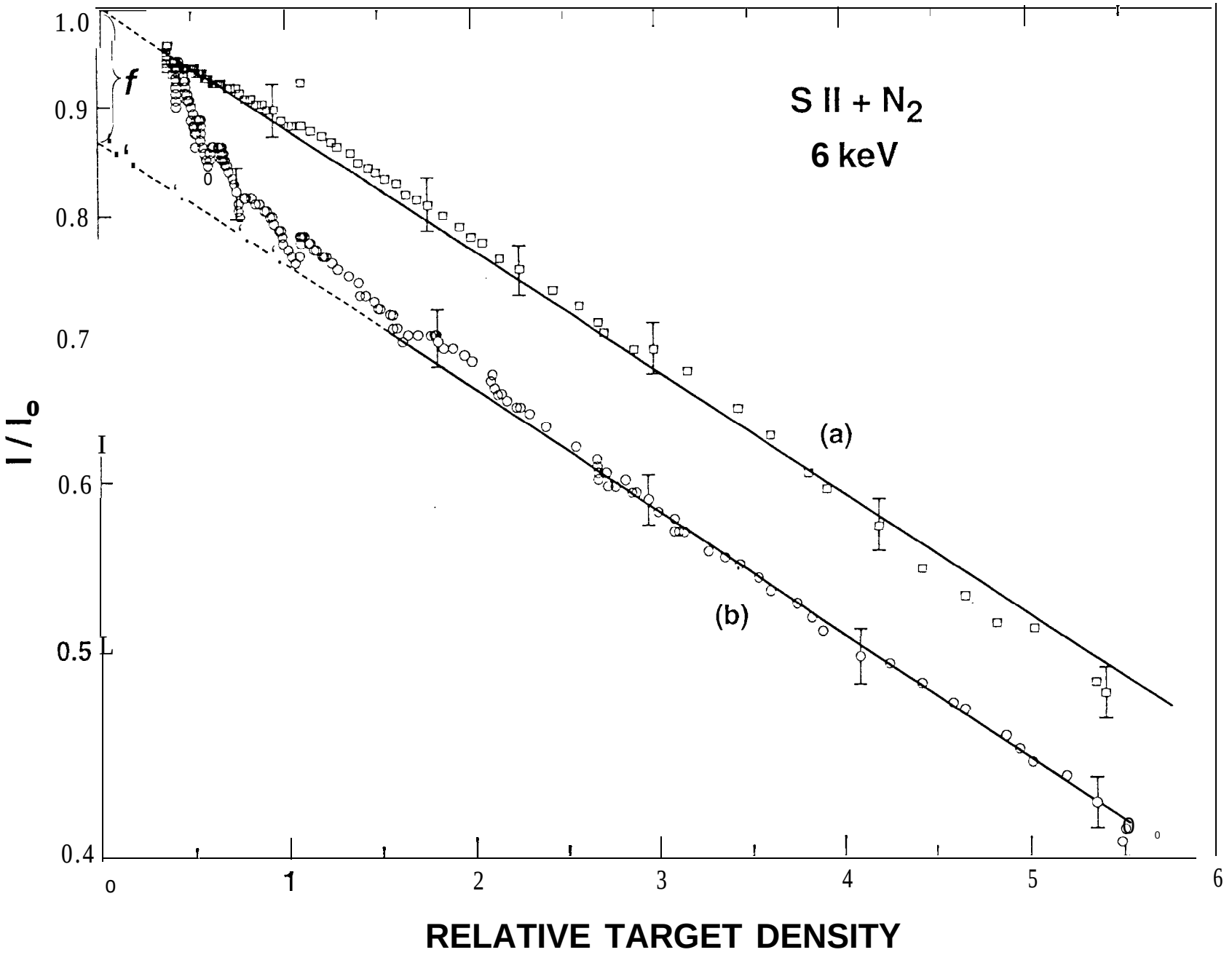
S II + N2
6 keV
f
(a)
(b)
I / I0
RELATIVE TARGET DENSITY
1.0
0.9
0.8
0.7
0.6
0.5
0.4
0
1
2
3
4
5
6

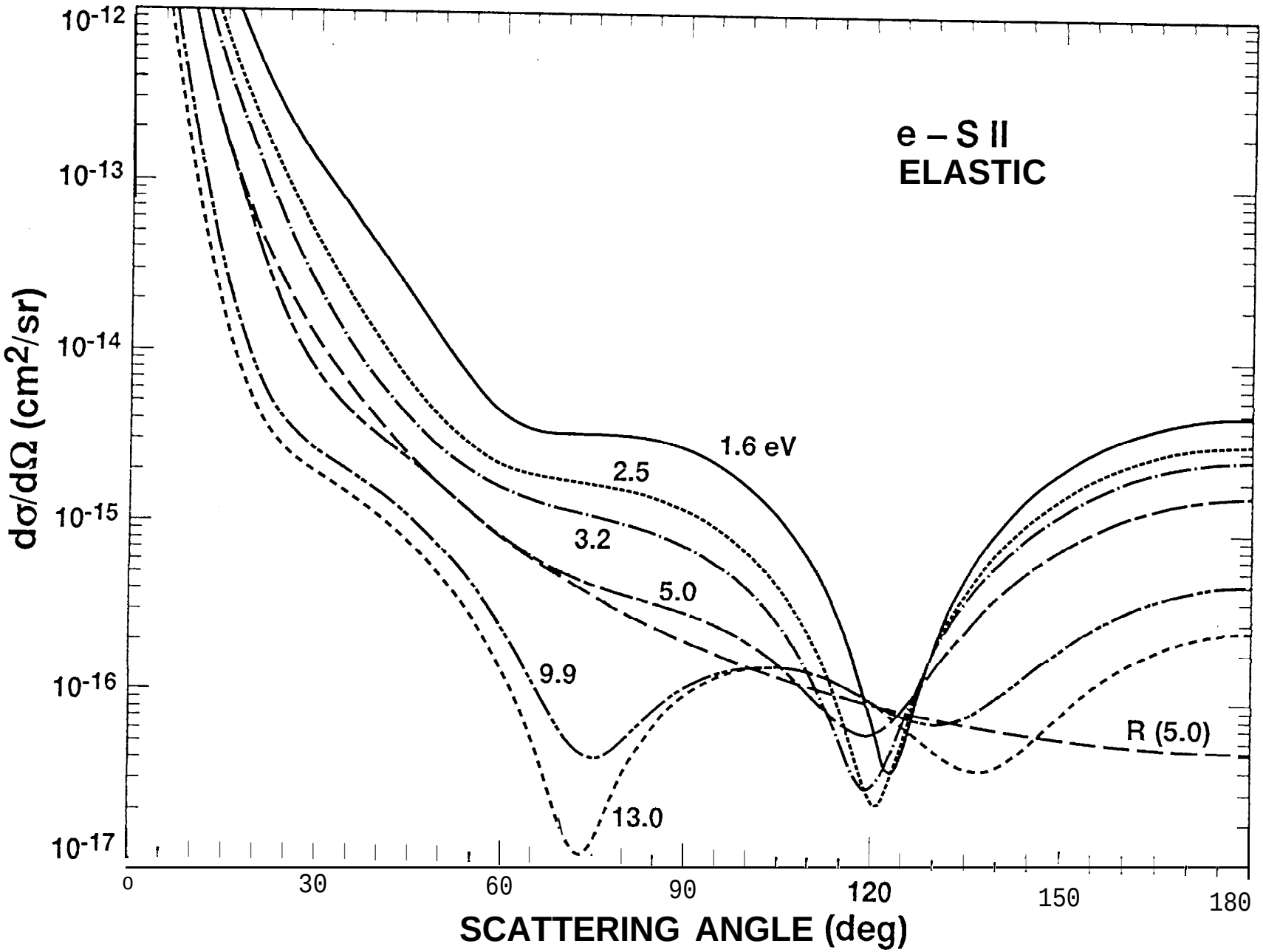
e – S II
ELASTIC
1.6 eV
2.5
3.2
5.0
9.9
13.0
R (5.0)
dσ/dΩ (cm²/sr)
10⁻¹²
10⁻¹³
10⁻¹⁴
10⁻¹⁵
10⁻¹⁶
10⁻¹⁷
0
30
60
90
120
150
180
SCATTERING ANGLE (deg)

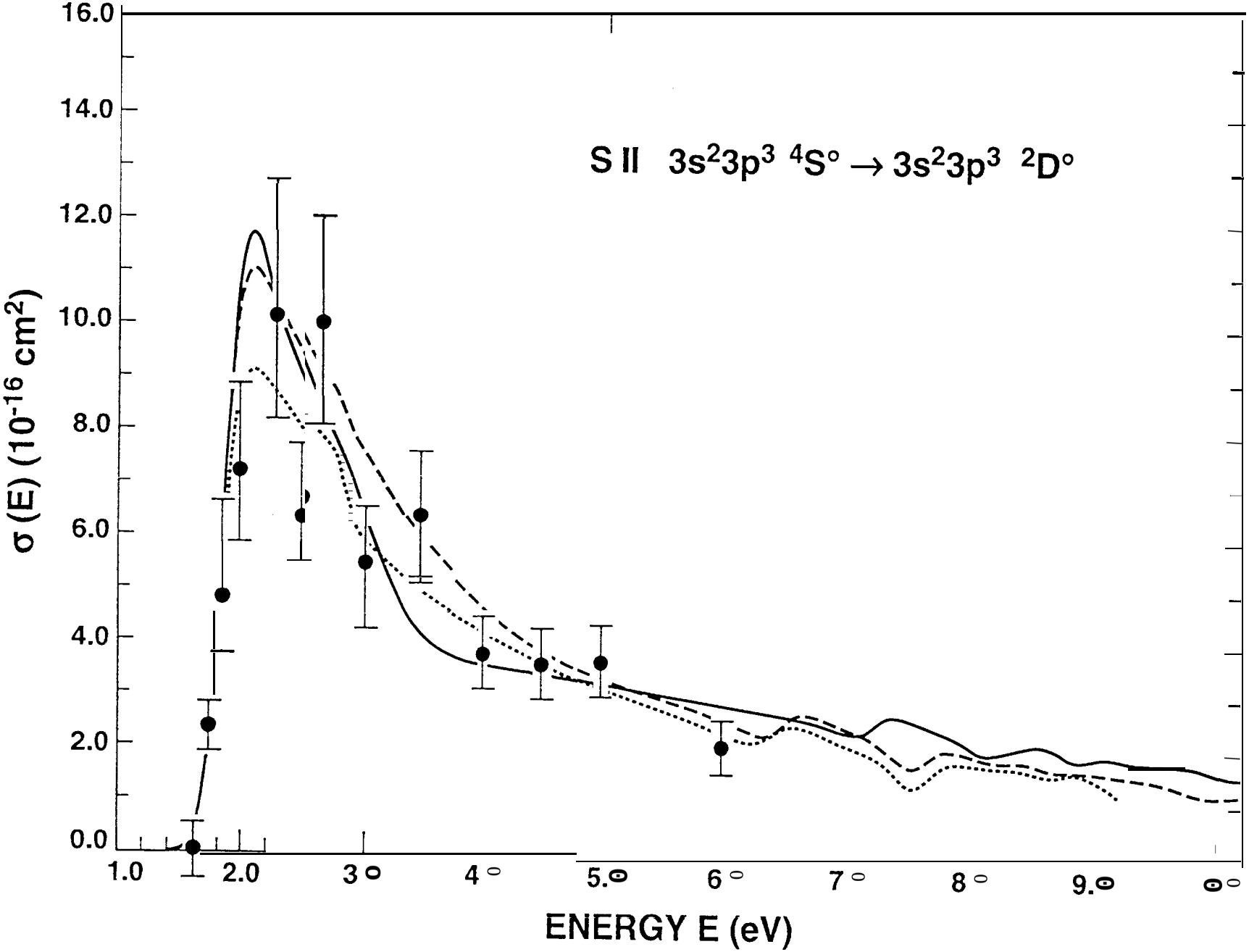
S II 3s²3p³ ⁴S° → 3s²3p³ ²D°
σ (E) (10⁻¹⁶ cm²)
ENERGY E (eV)
16.0
14.0
12.0
10.0
8.0
6.0
4.0
2.0
0.0
1.0
2.0
3.0
4.0
5.0
6.0
7.0
8.0
9.0

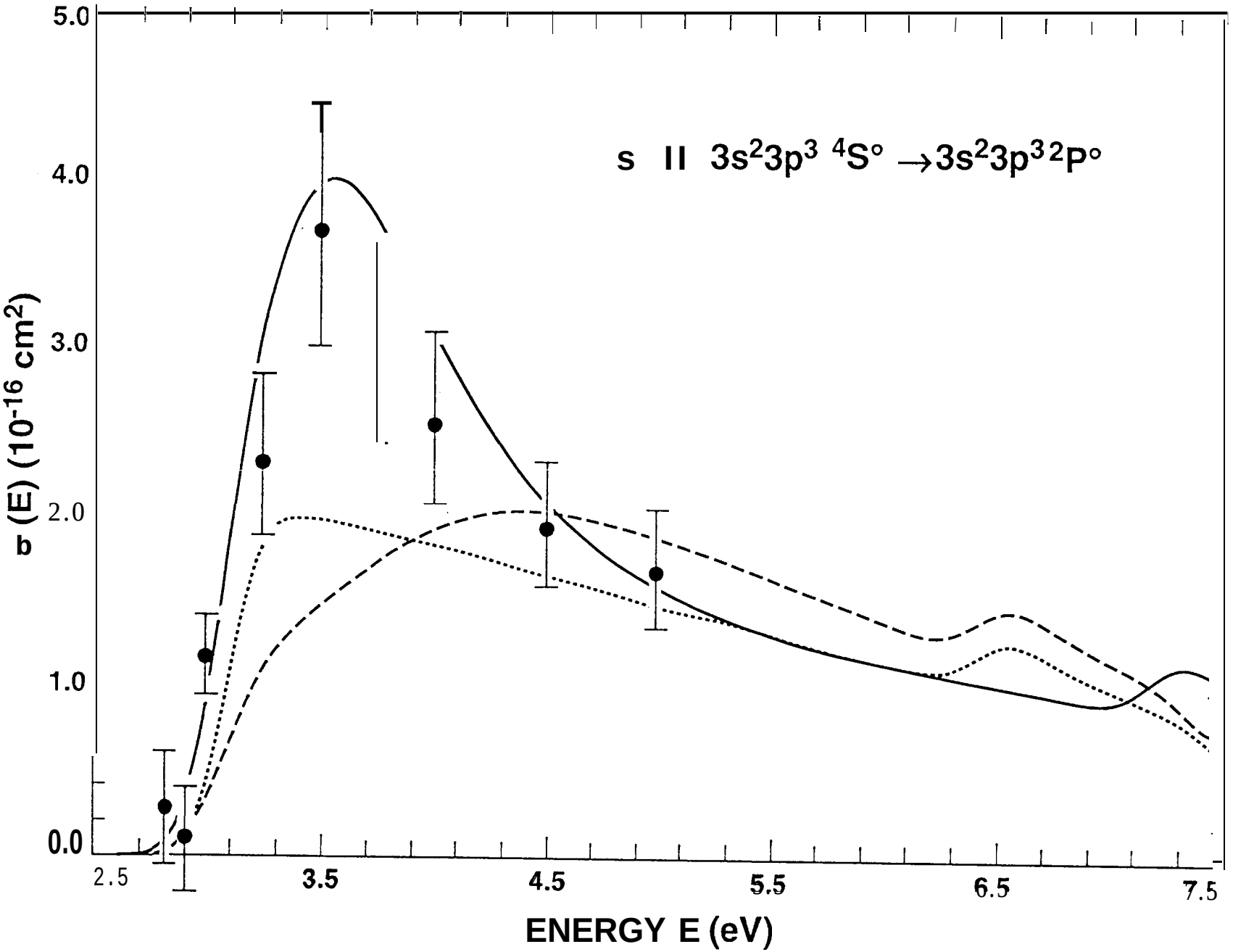
s II 3s²3p³ ⁴S° →3s²3p³ ²P°
σ (E) (10⁻¹⁶ cm²)
5.0
4.0
3.0
2.0
1.0
0.0
2.5
3.5
4.5
5.5
6.5
7.5
ENERGY E (eV)

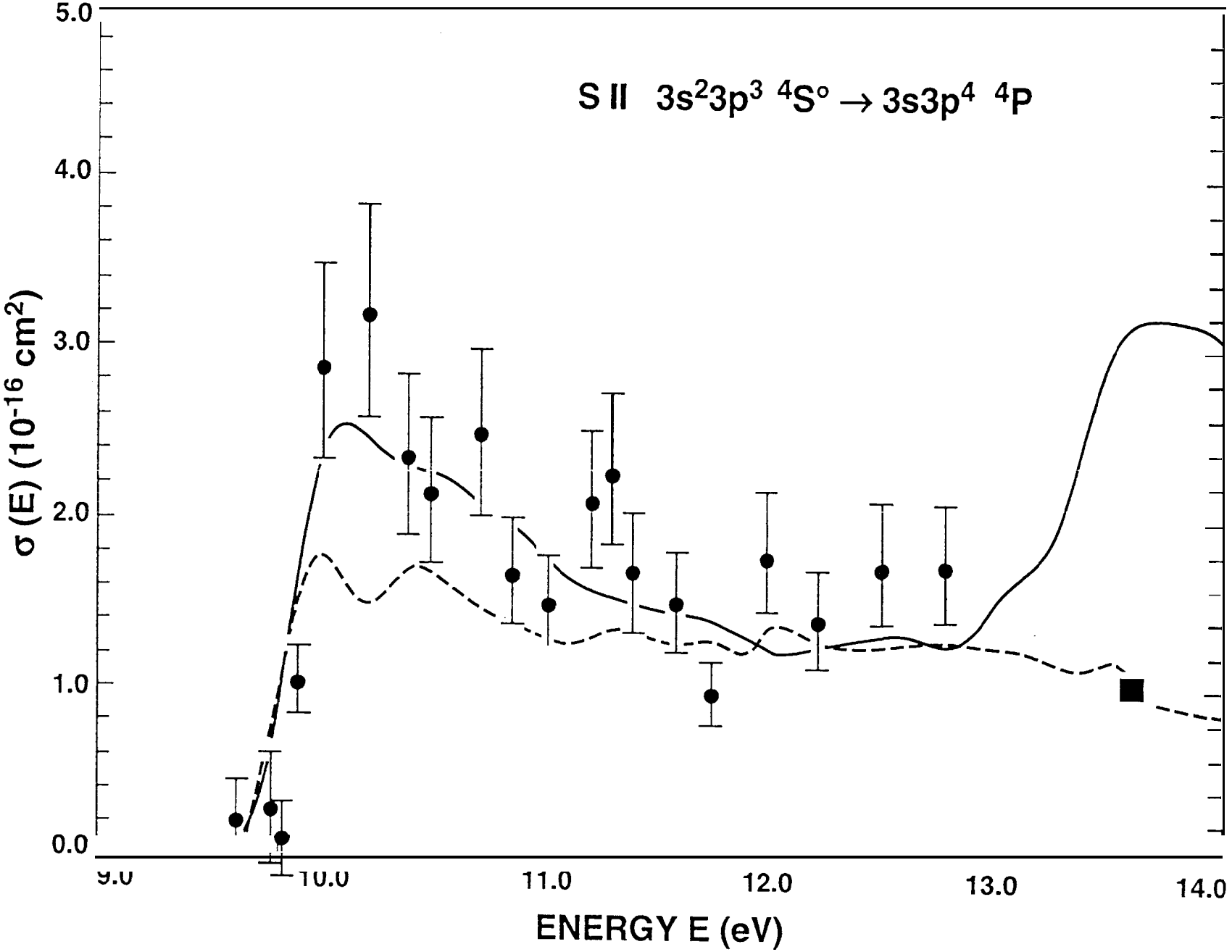
S II 3s²3p³ ⁴S° → 3s3p⁴ ⁴P
σ (E) (10⁻¹⁶ cm²)
5.0
4.0
3.0
2.0
1.0
0.0
9.0
10.0
11.0
12.0
13.0
14.0
ENERGY E (eV)